Nanoscale

RSC Publishing

PAPER

View Article Online
View Journal | View Issue

Cite this: *Nanoscale*, 2013, **5**, 2745

Co-axial electrospun polystyrene/polyurethane fibres for oil collection from water surface†

Jinyou Lin,[abcd] Feng Tian,[b] Yanwei Shang,[acd] Fujun Wang,[d] Bin Ding,*[ac] Jianyong Yu*[c] and Zhi Guo[b]

The pollution arising from oil spills is a matter of great concern due to its damaging impacts on the ecological environment, which has created a tremendous need to find more efficient materials for oil spill cleanup. In this work, we reported a sorbent for oil soak-up from a water surface with a high sorption capacity, good selectivity, and excellent reusability based on the hydrophobic–oleophilic fibrous mats that were fabricated *via* co-axial electrospinning polystyrene (PS) solution as the shell solution and polyurethane (PU) solution as the core solution. The fine structures of as-prepared fibers were regulated by manipulating the spinning voltages, core solution concentrations, and solvent compositions in shell solutions, which were also characterized by field emission scanning electron microscopy, transmission electron microscopy, nitrogen adsorption method, and synchrotron radiation small-angle X-ray scattering. The effects of inter-fiber voids and intra-fiber porosity on oil sorption capacities were well studied. A comparison of oil sorption capacity for the single fiber with different porous structures was also investigated with the help of scanning transmission X-ray microscopy. The results showed that the sorption capacities of the as-prepared sorbent with regards to motor oil and sunflower seed oil can be 64.40 and 47.48 g g^{-1}, respectively, approximately 2–3 times that of conventional polypropylene (PP) fibers for these two same oils. Even after five sorption cycles, a comparable oil sorption capacity with PP fibers was still maintained, exhibiting an excellent reusability. We believe that the composite PS–PU fibrous mats have a great potential application in wastewater treatment, oil accident remediation and environmental protection.

Received 9th December 2012
Accepted 3rd January 2013

DOI: 10.1039/c3nr34008b

www.rsc.org/nanoscale

Introduction

Oil plays a very important role in the modern industrial world. It is a necessity for a great number of chemicals and synthetic polymers.[1,2] Unfortunately, oil accidents often occur as a result of its exploitation, transportation, utilization, storage, *etc.*, resulting in not only energy loss but also threats to the environment.[1,3] When oil spills on water, it forms an emulsion or floating film. If the spilled oil is not treated in time, its discharge into the environment can be toxic to various microorganisms.[4] Furthermore, sewers containing mineral oil or fuel carried from the streets by rain and water polluted with edible oils after continuous washing-up in restaurants are also problems that must be dealt with.[5] Therefore, it is imperative that effective countermeasures should be adopted to treat oil spills, petroleum products, as well as the discarded edible oils.

Among the various methods of oil spill cleanup, including physical methods (*i.e.*, sorbents, booms, and skimmers), chemical methods (*i.e.*, *in situ* burning, and using of solidifiers) and bioremediation, mechanical recovery of oil by sorbents is one of the most promising methods.[6] This process involves using a sorbent to concentrate and transform liquid oil to a semisolid or solid phase that can be removed from temporary storage with the help of oil sorbents.[3,7] As a result, a good hydrophobicity–oleophilicity, a high uptake capacity, a high rate of uptake, and good buoyancy are required for an ideal sorbent material for oil spill cleanup.[8]

Over the past two decades, the sorbents used for oil sorption mainly included natural materials, inorganic mineral products,

[a]*State Key Laboratory for Modification of Chemical Fibers and Polymer Materials, College of Materials Science and Engineering, Donghua University, Shanghai 201620, China. E-mail: binding@dhu.edu.cn; Fax: +86-21-62378202; Tel: +86-21-62378202*

[b]*Shanghai Institute of Applied Physics, Chinese Academy of Sciences, Shanghai 201204, China*

[c]*Nanomaterials Research Center, Research Institute of Donghua University, Shanghai 200051, China. E-mail: yujy@dhu.edu.cn*

[d]*College of Textiles, Donghua University, Shanghai 201620, China*

† Electronic supplementary information (ESI) available: FE-SEM images in high resolution of the samples formed at different conditions (Fig. S1). Nitrogen adsorption–desorption isotherm and FE-SEM image (inset) of the conventional PP fibers (Fig. S2). FT-TR spectra of the selected fibrous mats formed with different conditions (Fig. S3). Oleophilicity–hydrophobicity of the composite PS–PU fibrous mat (Fig. S4). A dynamic process of oil cleanup from the water surface by using the composite PS–PU fibrous mat (Fig. S5). Optical images of the electrospun composite PS–PU fibrous mats (Fig. S6). Mechanical properties of the electrospun composite PS–PU fibrous mats (Table S1). See DOI: 10.1039/c3nr34008b

and organic synthetic fibers.[3] Among these sorbent materials, non-woven polypropylene (PP) fibers, as synthetic fibers, have been widely used as sorbents in oil cleanup due to their hydrophobic–oleophilic properties, good oil–water selectivity, high buoyancy, and scalable fabrication. However, they suffered from a low oil sorption capacity (15–30 g g^{-1}) because of their low porosity and solid fibers with large diameters.[3,9]

In recent years, various nanostructures in the form of nanoparticles, nanofibers, nanowires, nanobelts and nanotubes have been created as a result of the developments of nanoscience and nanotechnology.[10,11] An appropriate post-treatment through the use of a non-polar material with low surface energy on these nanomaterials enabled them to exhibit hydrophobicity–oleophilicity properties, which rendered these materials particularly suited for applications in oil cleanup from water.[12–17] Electrospinning, an efficient and simple method for generating polymeric fibers with diameters both on the micro- and nanoscales, has gained increasing attention as it can not only control the fiber diameter easily but can also manipulate the individual fiber structures *via* variable tuning.[18–22] More recently, electrospun fibers were used as oil sorbents, which showed many advantages compared to the conventional PP fibers.[23,24] It is believed that the oil sorption capacity will be increased if the fibrous sorbent has the capability of driving the oil not only into the voids among fibers but also into the interiors of fibers. Hence, we investigated the effect of fine structures and the specific surface area (SSA) of electrospun polystyrene (PS) fibers on their oil sorption capacities.[25]

However, one fatal problem of electrospun fibers used as oil sorbents is the reduction in fiber strength and resiliency after oil sorption, which results in poor reusability. Fortunately, the core–shell configuration of fibers *via* co-axial electrospinning provides the potential for achieving unique properties from a product that are difficult to obtain from the constituent materials if spun separately.[26] It is well known that electrospun polyurethane (PU) fibers have a good strength and elasticity.[27] Thus, in this study, we report a composite PS–PU fiber with a high SSA prepared *via* co-axial electrospinning directly for use as an oil sorbent. The effects of applied voltages, core solution concentrations, and solvent compositions in shell solution on fiber morphology and their fine structures were extensively studied. The oil sorption capacities of as-prepared composite PS–PU fibrous mats for motor oil and sunflower oil as well as their influencing factors were investigated and well discussed. In addition, the oil retention, possible reusability, and tensile property of as-spun oil sorbents were also evaluated.

Experimental

Materials and preparation of fibrous mats

The materials used in this study include polystyrene (PS) (M_w = 350 000 g mol^{-1}, Aldrich), tetrahydrofuran (THF) and *N*,*N*-dimethylformamide (DMF) (Shanghai Chemical Reagents Co., Ltd, China). The polyurethane (PU) resin was kindly obtained from Suzhou Baoze Polymer Co., Ltd., China. The oils used for adsorption are motor oil (Shanghai RuiBei SINOPEC Co., Ltd., China) and sunflower seed oil (Standard foods China Co., Ltd., China). The iron acetylacetonate and the PP non-woven fibrous mats were purchased from Aladdin Chemistry Co. Ltd. and Shandong HuaYe Nonwoven Fabric Co., Ltd., China, respectively.

The 20 wt% PS solutions were prepared by dissolving PS in solvent mixtures of THF–DMF with weight ratios of 1 : 3 and 1 : 4, respectively, and in DMF solvent only. The PU resin was diluted to 75 and 50 wt%, respectively, in spinning solutions by adding DMF. The schematic of the co-axial electrospinning setup used in this study was shown in Fig. 1, which was produced by Shanghai Oriental Flying Nanotechnology Co., Ltd., China. The solutions for the core and shell materials were separately fed into the co-axial nozzle from which they were ejected simultaneously by utilizing one syringe pump. The spinneret connected with a syringe pump was fixed to a support that could be moved with a speed of 10 m min^{-1} along the slipway paralleled to the rotating roller with a linear velocity of 30 m min^{-1}. All the fibrous mats were prepared in a relative humidity of 40% at 24 °C at a solution feed rate of 4 mL h^{-1} and with a constant work distance of 15 cm between the spinneret and collector.

Characterizations of polymer solutions and fibrous mats

The viscosity of polymer solutions was determined by using a rotational viscometer (NDJ-79, Shanghai Changji Geological Instruments Co., Ltd China), and the results are shown in Table 1.

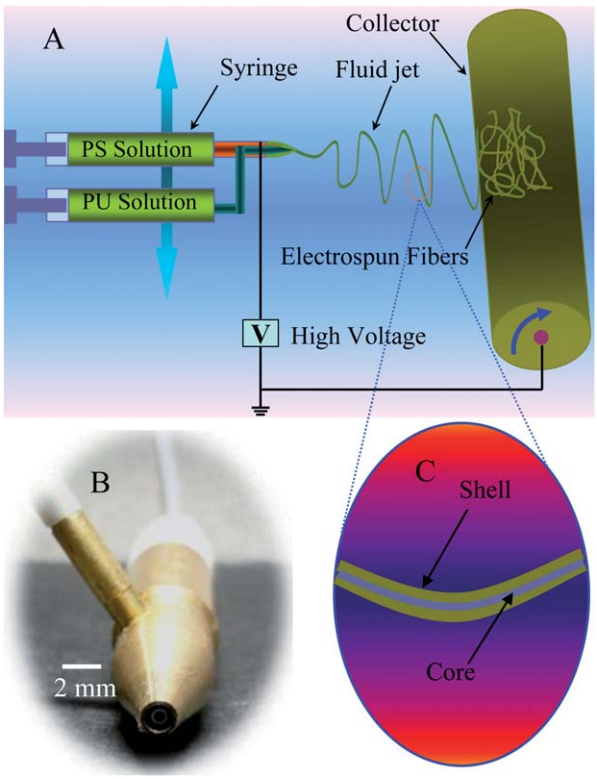

Fig. 1 (A) Schematic representation showing the core–shell electrospinning setup used in this study. (B) Photograph of the co-axial spinneret. (C) An illustration of the electrospun core–shell fiber.

Table 1 Viscosity of the solutions

Solutions	Viscosity (Pa s)
Initial PU resin (solid content: 40%)	15
75 wt% PU resin	2.4
50 wt% PU resin	0.290
20 wt% PS (THF/DMF = 1 : 3, w/w)	0.242
20 wt% PS (THF/DMF = 1 : 4, w/w)	0.250
20 wt% PS (DMF)	0.265

The morphology of electrospun composite PS–PU fibers was examined by a field emission scanning electron microscope (FE-SEM) (S-4800, Hitachi Ltd, Japan). A transmission electron microscope (TEM) (H-800, Hitachi Ltd, Japan) was used to study the internal morphology of as-prepared fibers. The surface topography of fibrous mats was assessed by non-contact profilometry using an interferometer profiler (Wyko-Veeco, model NT9100, USA). Adsorption measurements using a sample mass no less than 0.4 g were performed on a Micromeritics ASAP 2020 volumetric adsorption apparatus (USA). The SSA of the as-spun fibrous mats were obtained from nitrogen adsorption data in the relative pressure range from 0.03 to 0.35 by using the Brunauer–Emmett–Teller (BET) method. The pore size distributions of fibrous mats were calculated from the desorption branch of the nitrogen adsorption data using the Barrett–Joyner–Halenda (BJH) method. The fine structures of the as-spun fibers were also characterized by synchrotron radiation small-angle X-ray scattering (SAXS) at Beamline BL16B1 of the Shanghai Synchrotron Radiation Facility (SSRF). Fourier transform infrared (FT-IR) spectra of selected fibrous mats were recorded with a Nicolet 8700 FT-spectrometer.

The tensile property of the as-prepared fibrous mats was tested on a tensile test apparatus (LLY-06E, Laizhou Electron Instrument Co., China) with a cross-head speed of 10 mm min^{-1} at constant temperature (25 °C) and humidity (40%). The sample was prepared with 10 mm in length and 5 mm in width *via* die cutting from the fibrous mats. The thickness of samples was evaluated by an YG-141N fabric thickness gauge (Nantong Hongda Experiment Instruments Co., Ltd., China) for five times independently, and the average value was obtained. The tensile stress and extension of these fibrous mats were calculated as in our previous study.[28]

Oil sorption evaluation of as-prepared fibrous mats

All of the oil sorption measurements were conducted at 25 °C. An artificial oil–water bath was formed by adding 20 g oil into a 250 mL beaker containing 150 mL water. Approximately 0.1 g of sorbent was put onto the oil layer, and the sorption behavior was recorded by a conventional digital camera over time. The oil sorption capacity for the sorbent was obtained from the following equation:

$$Q = \frac{m_0 - m_s}{m_s} \quad (1)$$

where Q is the oil sorption capacity (g g^{-1}), m_0 is the total mass of wet sorbent after drained, and m_s is the initial mass of sorbent (g). The wet sorbent was taken out using a nipper, drained for 1 min and then weighed. For each sample, the measurement was repeated three times independently, and the average value and standard deviation were calculated. The sorbent with oil was squeezed by padding paper at a maximum pressure to remove the sorbed oil. Subsequently, the squeezed sorbent was subjected to the same procedures of measurement for oil sorption capacity as described above to determine its reusability. Moreover, the rate of oil desorption from sorbed sorbent by gravity was also examined over time according to the previous report.[2]

The single fiber with different porous structures was immersed into the sunflower seed oil with an addition of 0.5 wt % iron acetylacetonate to get a sufficient sorption. The absorption contrast images of the single fiber taken from different samples at the iron absorption and pre-absorption edges energy (708.7 eV and 704 eV) was performed on the scanning transmission X-ray microscope (STXM) BL08U1A at SSRF. The distribution of iron within the as-prepared single fiber was calculated by using the software of Dual Energy Element Distribution.[29] From the iron element distribution within the different single fiber, we can assess the effect of porous structures on its oil sorption capacity qualitatively.

Results and discussion

Morphology of the composite PS–PU fibers

Fig. 2a and b show the FE-SEM images of electrospun composite PS–PU fibers prepared *via* co-axial electrospinning at different applied voltages. As can be seen, the resultant electrospun fibers randomly orientate in a form of non-woven mats with a three dimensional (3D) porous structure. The composite PS–PU fibers have a ribbon-like configuration with an average width of 8 μm and extreme lengths of several hundred micrometers (Fig. 2a and b). During the process of co-axial electrospinning,

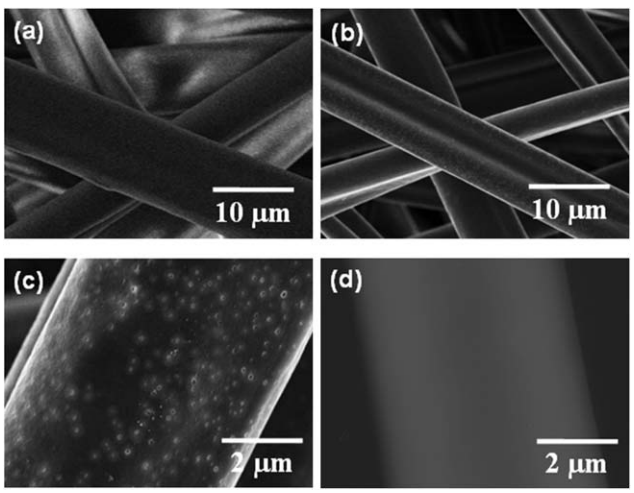

Fig. 2 (a) FE-SEM images of the composite PS–PU fibers formed at (a) 20 and (b) 25 kV. (c) High magnification SEM image and (d) TEM image of the fiber formed at 25 kV. (A 20 wt% PS dissolved in 1 : 4 THF/DMF was used as the shell solution and the initial PU resin was used as the core solution.)

the solvent used for shell solution is the mixture of THF–DMF with a weight ratio of 1 : 4 which has a much higher solvent volatility than that of a sole solvent of DMF used in core solution exhibiting a relatively high viscosity (Table 1). Therefore, the rate of solvent removal from the charged fluid jet on its surface is larger than that of the solvent diffusion rate inside the jet. In this case, the atmospheric pressure tends to collapse the charged fluid jet to form a ribbon-like fiber.[30]

It is interesting to note that the composite PS–PU fibers formed at 25 kV are covered with numerous nanopores on their surfaces, exhibiting highly porous surfaces as shown in Fig. 2b and c, an image of the surface pores in high magnification was shown in Fig. S1a.† However, the fibers prepared at 20 kV show very smooth surfaces. In this co-axial electrospinning, the composite fluid jet ejects from the needle tip, the core solution with a high elasticity should be encapsulated by the PS solution with a poor elasticity. A porous layer with a smooth surface was formed due to the competition between the phase separation and the solidification of the PS solution on the surface layer of composite jet. This observation agreed very well with our previous study that the pure electrospun PS fibers exhibited highly porous cores with very smooth surfaces.[25] Therefore, if the shell solution is insufficient to encapsulate the core solution, the imperfect core–shell structure will be formed. This was confirmed by the TEM image of as-prepared fiber (Fig. 2d), which was ascribed to the large viscosity difference between these two kinds of polymer solutions (Table 1). In such a case, a stronger stretching acting on the composite jet generated by a much higher applied voltage (25 kV) will enable the porous PS layer with smooth surfaces to be damaged and uncontinuous, leading to the formation of nanopores on the fiber surfaces (Fig. 2c).

To reduce the viscosity difference between the core solution and the shell solution, the initial PU resin was diluted to 75 and 50 wt%, respectively, by adding the solvent of DMF. Fig. 3a and c show the FE-SEM images of composite PS–PU fibers formed with different PU solutions as the core solutions. It can be seen that the average fiber width (or diameter) is continuously decreased with the decreasing of core solution concentrations and the fiber shape is changed gradually from ribbon-like to circular. This is attributed to the lower viscosity of core solutions used in electrospinning that strengthened jet instability and changed the competition between the solvent removal rate from jet surface and the solvent diffusion rate inside the jet.[28,30] High magnification images of the samples shown in Fig. 3a and c show that there are no nanopores on fiber surfaces (Fig. 3b and d, further details can be seen Fig. S1b†). This result could be ascribed to the increase of PS within the composite fiber, which enabled the thickness of the shell layer (PS) to be increased.

To confirm the existence of a core–shell structure within the as-prepared fibers, internal structures of these fibers were examined by TEM. It was found that the 75 wt% PU resin used as the core solution was still too high to form a core–shell structure. (The TEM image was not shown.) Fig. 3e shows the TEM image of the composite PS–PU fiber prepared with a 50 wt% PU resin as the core solution, revealing a perfect core–shell structure is successfully achieved. As can be seen, the thickness of the PS layer is not very thick according to the red arrow marked in Fig. 3e due to the relatively less amount of PS within the composite fiber. The blue arrow marked in Fig. 3f indicates that the fiber has a porous surface layer. Therefore, it is believed that the shell of the as-prepared fibers is also porous rather than solid.

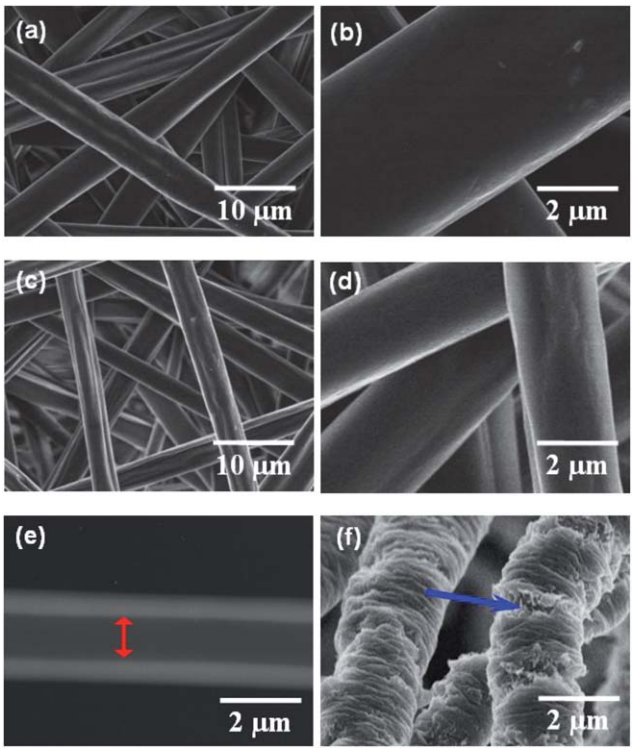

Fig. 3 FE-SEM images of the composite PS–PU fibers formed with (a) 75 and (c) 50 wt% PU solutions as the core solutions. (b) and (d) show the high magnification images of the samples shown in (a) and (c), respectively. (e) TEM image of as-spun fiber shown in (c). (f) FE-SEM image of fibers shown in (c) after stretching. (A 20 wt% PS dissolved in 1 : 4 THF/DMF was used as the shell solution; the applied voltage was kept at 25 kV.)

To investigate the effect of solvent compositions in shell solution on the morphology of as-prepared fibers, a 50 wt% PU resin was selected as the core solution. Fig. 4a and b show the FE-SEM images of composite PS–PU fibers formed with a 20 wt% PS dissolved in 1 : 3 THF/DMF as the shell solution. As shown in Fig. 4a, the fiber diameter displays no obvious change in comparison with the fibers described in Fig. 3c, which is attributed to the same concentration of shell solutions with a comparable solution viscosity (Table 1). However, a high magnification image of the fibers shows that many nanopores are present on the fiber surfaces (indicated by a dotted circle, Fig. 4b and S1c†), which agrees well with the supposition that the high volatility solvent can create nanopores on fiber surfaces.[24,31]

In co-axial electrospinning, a stable jet ejected from the apex of the composite Taylor cone is essential for the formation of core–shell fibers.[26] A high applied voltage or a spinning solution with high conductivity will enable the Taylor cone at the tip of the spinneret to be unstable or to recede into the spinneret,[32] as a result, the multi-jets will be formed from the Taylor cone, which is unfavorable to the formation of core–shell fibers.[26] DMF is the solvent with a high dielectric constant, in which the

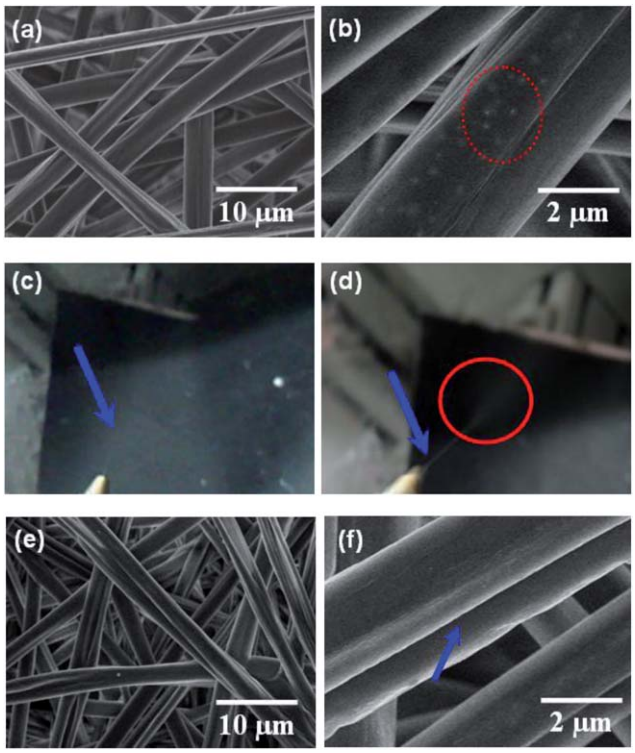

Fig. 4 FE-SEM images of the composite PS–PU fibers formed with (a) a 20 wt% PS dissolved in 1 : 3 THF/DMF and (e) a 20 wt% PS dissolved in pure DMF as the shell solutions. (b) and (f) show the high magnification images of the samples shown in (a) and (e), respectively. Optical images of the electrospinning process at (c) 25 and (d) 20 kV. (A 50 wt% PU solution was used as the core solution and the applied voltage was kept at 25 and 20 kV for the samples prepared shown in (a) and (e), respectively.)

solution shows a relatively high conductivity.[33] Fig. 4c shows the optical image of the co-axial electrospinning process at 25 kV, revealing that the composite Taylor cone is unstable and the multi-jets are formed from the spinneret directly as marked by the blue arrow.

Therefore, to obtain the stale jet from the Taylor cone, the applied voltage was decreased to 20 kV as shown in Fig. 4d, which shows that a stable jet formed from the spinneret and followed a direct path towards the grounded target for a very short distance from its origin and then became unstable as marked by the blue arrow and red circle. Fig. 4e and f show the FE-SEM images of composite PS–PU fibers formed with a 20 wt% PS dissolved in pure DMF as the shell solution at 20 kV. As can be noted, the fibers have large trenches on their surfaces along the fiber axial with a few tens of nanometers both in width and depth. Furthermore, there are many nanopores presented on the fiber surfaces with shallow depth (Fig. S1d†). The typical fiber morphology of these fibers can be ascribed to the easy occurrence of bulk instability on the composite fluid jet when a high conductivity shell solution was utilized.[34]

Porous structure of the composite PS–PU fibers

In our previous reports,[31,35,36] we have demonstrated that the electrospun PS fibers formed from the solvent mixtures of THF–DMF with a high content of DMF have smooth surfaces and highly porous interiors which enabled the resultant fibers to show a high SSA. It is expected that these composite microfibers prepared *via* co-axial electrospinning also have a high SSA. Fig. 5a shows the nitrogen adsorption–desorption isotherms of composite PS–PU fibrous mats. It can be observed that these composite PS–PU fibrous mats have large quantities adsorbed of nitrogen, above 28 g cm^{-3}, of which the highest value can reach up to 90.14 g cm^{-3}. However, the conventional PP fibers with an average diameter of 18 μm and nonporous structure only show a quantity adsorbed of nitrogen 0.31 g cm^{-3} as displayed in Fig. S2.† From the BET measurements (Table 2), it can be found that the SSA of these PS–PU fibrous mats showed a highest value of 19.57 m^2 g^{-1}, whereas the PP fibers showed a SSA of 0.35 m^2 g^{-1} (Fig. S2†), indicating an increase of at least a factor of 55.

If the electrospun fibers are solid without a porous structure and have a very small SSA, in particular the fiber diameters are larger than 4 μm.[24,37] The solid PP fibers, only showing a SSA of 0.35 m^2 g^{-1}, also confirmed this result. It is reasonable to conclude that the composite PS–PU microfibers are porous

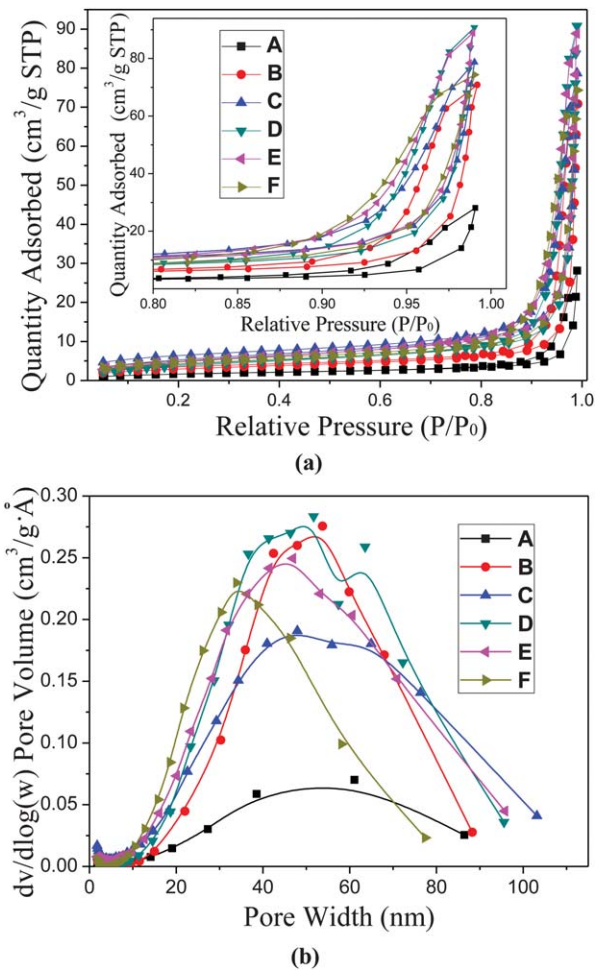

Fig. 5 (a) Nitrogen adsorption–desorption isotherms of the composite PS–PU fibrous mats. (b) Pore size distribution curves of the composite PS–PU fibrous mats calculated from the desorption branch by using BJH method. (The samples A to F are the corresponding fibers shown in Table 2.)

Table 2 Characterization of the porous structures within the electrospun composite PS–PU fibers

Samples	Applied voltages (kV)	Core solutions (wt% PU)	DMF/THF in shell solutions	SSA[a] ($m^2\ g^{-1}$)	TPV[b] (cm^3/g)	APW[c] (nm)
A	20	100	1 : 4	6.10	0.043	29.27
B	25	100	1 : 4	10.99	0.109	37.91
C	25	75	1 : 4	15.02	0.120	34.37
D	25	50	1 : 4	19.57	0.139	24.47
E	25	50	1 : 3	18.43	0.138	28.25
F	20	50	1 : 0	15.72	0.114	27.79

[a] SSA was calculated by the BET method. [b] TPV indicates total pore volume, which was calculated by the BJH method from the desorption branch of nitrogen physisorption isotherm. [c] APW indicates BJH desorption average pore width.

rather than solid, otherwise, it is impossible for them to show such a large quantity of adsorbed nitrogen. The isotherms, as displayed in Fig. 4a, can be categorized as type II with a hysteresis loop, which is characteristic of mesopores (2–50 nm pore width) and macropores (>50 nm pore width) according to the International Union and Applied Chemistry (IUPAC) classification.[38] The sharply increased quantity of adsorbed N_2 at a high relative pressure (>0.8 P/P_0) is attributable to the macropores and mesopores of as-prepared fibers. Fig. 5b illustrates that the pores of the composite PS–PU fibers are in the range of 20–100 nm, which agrees well with the N_2 physisorption isotherm data as well as the observation of FE-SEM image as shown in Fig. 2c.

The fibers formed from initial PU resin as the core solution at 25 kV show a SSA and TPV of 10.99 $m^2\ g^{-1}$ and 0.109 $cm^3\ g^{-1}$, respectively, which are much higher than those of fibers formed at 20 kV (Table 2). This indicates that the high stretching created by a high spinning voltage in electrospinning results in the formation of a much more porous structure within the composite fibers, which is in accordance with the FE-SEM images as shown in Fig. 2. Moreover, with the decreasing of core solution concentration, both the SSA and total pore volume (TPV) are increased due to the increasing thickness of the porous PS layers with decreasing core concentration (Table 2). Because of the decreasing fiber diameter, the average pore width (APW) is decreased from 37.91 to 24.47 nm as the core solution concentration decreases, indicating that these pores are intra-fiber pores rather than inter-fiber voids. Additionally, both the SSA and TPV of the as-prepared fibers formed with the same core solution show a unimodal distribution with the changing of solvent composition, while the APW shows a little variation. The results show that the composite PS–PU microfibers prepared *via* co-axial electrospinning have porous structures within the fibers.

SAXS is a technique to probe the nanoscale structure and fluctuations in soft matter.[39] To further investigate the porous structure within as-prepared fibers, the SAXS measurements were conducted at Beamline BL16B1 of the SSRF. Fig. 6a presents the corresponding two dimensional (2D) SAXS patterns showing a circular shape, which indicates the random orientation both nanofibers and the nanoscale structure within the fibers. More interestingly, the pattern shape of the sample A is smaller than that of the sample B, which can be explained by the presence of the much smaller TPV within fibers of the sample A. It is believed that the mesopores and macropores within the fibers enhance the intensity of X-ray scattering. The pattern shapes of samples B to D are gradually enlarged with the decreasing of core solution concentration due to the increasing of TPV. The pattern shape of sample F is also smaller than that

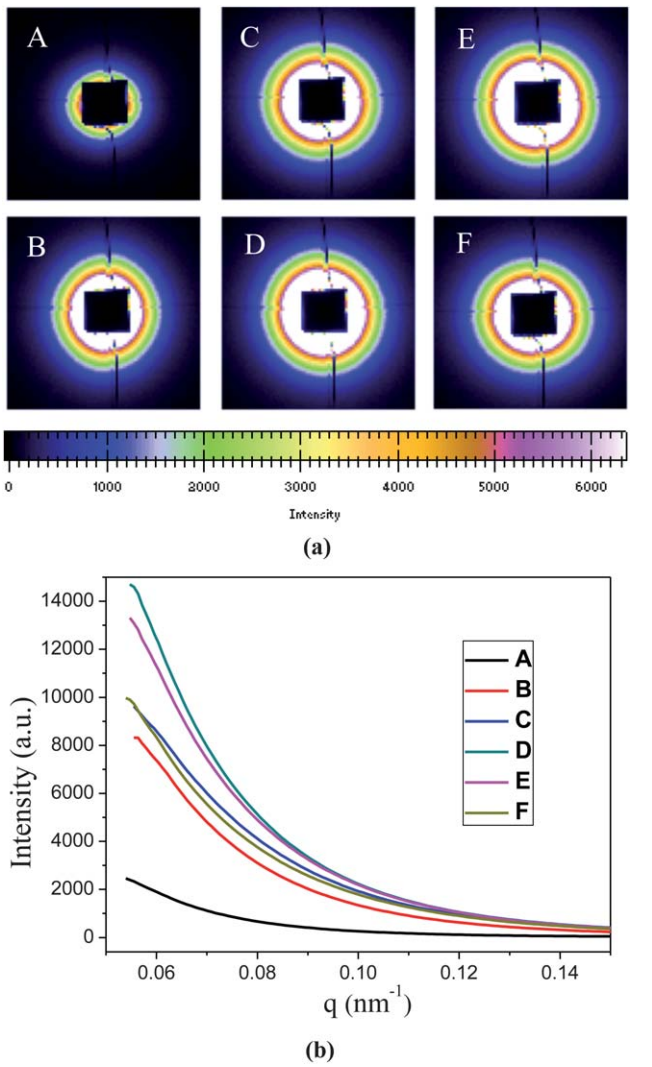

Fig. 6 (a) SAXS 2D scattering patterns and (b) SAXS curves of the composite PS–PU fibrous mats. (The samples A to F are the corresponding fibers shown in Table 2. Fit2D software was used to analyze the 2D SAXS data.)

of sample E but comparable to sample C, which is in good agreement with the variation of TPV of these samples (Table 2). From nitrogen absorption data, we found that the samples D and E have a very similar TPV, therefore, the pattern shapes of these two samples show no obvious difference. Fig. 6b shows the $I(q)$ *vs.* q curves of theses samples obtained for the 2D SAXS patterns, which clearly show the effect of a porous structure on X-ray scattering. These results agree very well with the characterization of the fiber porous structure by the nitrogen adsorption method.

Hydrophobicity–oleophilicity of the composite PS–PU fibrous mats

The hydrophobicity of as-prepared fibrous mats is closely related to their compositions. Fig. S3† shows the FT-IR spectra of the selected fibrous mats (pure PS fibrous mat, pure PU fibrous mat, and the composite fibrous mats formed with different core solutions when the shell solution was unchanged). As expected, the absorption peaks at 3060, 3026, 1600, 1493, 1452, and 757 cm^{-1} are assigned to the phenyl (Ph) group, the peaks at 2923 and 2850 cm^{-1} corresponded to the stretching vibration of CH and CH_2 groups on the main PS chain, the aromatic C–C out-of-plane bend at 699 cm^{-1}, and the C–Ph bond was at 1028 cm^{-1}.[40] The peaks of pure PU fibrous mat can be mainly assigned as: 3320 cm^{-1} (stretching of N–H groups), 2942 cm^{-1} (CH_2 asymmetric vibration), 2860 cm^{-1} (CH_3 symmetric vibration) 1705 cm^{-1} (C═O bond), 1532 cm^{-1} (urethane amide II), 1070 cm^{-1} C(O)–O–C stretching of the hard segment, and 817 cm^{-1} (bending vibration in benzene ring).[41] Both the peaks of the pure PS and the pure PU were detected within the composite PS–PU fibrous mats, which confirmed the successful fabrication of bicomponent composite fibrous mats composed of PS and PU matrices. Therefore, it is believed that the PS component contribute to the hydrophobicity of resultant fibrous mats.

Fig. 7a presents the optical image of water droplets on as-prepared fibrous mats (sample A was selected to study). As can be seen, the water droplets are stably placed on the as-prepared fibrous mats with an apparently obtuse contact angle. The 3D porous fibrous mat consisting of composite microfibers exhibits hierarchical structures on its surface layer with a high surface roughness value of 72.85 μm, reflecting that there are many large voids among these fibers (Fig. 7b), which enables much more air to be trapped under the water droplet as a cushion to support it. Combined with the low surface energy and nonpolarity of PS within the composite fibers, this typical structure contributes to a good hydrophobicity of the composite PS–PU fibrous mats.[35,40]

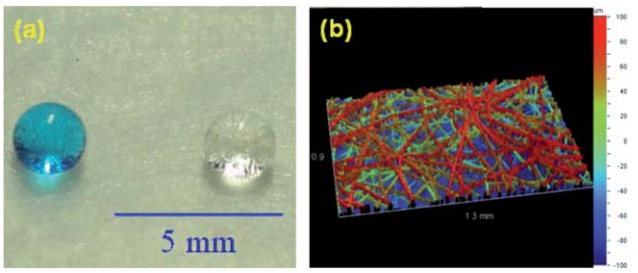

Fig. 7 (a) Optical image of water droplets on the as-prepared fibrous mat. (b) Optical profilometry image of the as-prepared fibrous mat. The water was labeled with blue color.

The good hydrophobicity–oleophilicity and the high rate of oil uptake are important properties for a good oil sorbent and should be considered for oil spill cleanup materials. These properties facilitate the oils to be soaked out conveniently and easily from the oil–water bath. To examine the rate of oil uptake of the as-prepared fibrous mats, a completely dynamic process of oil droplet which dripped from a needle tip and was placed on the fibrous mats was recorded by a conventional digital camera (Fig. S4†). It can be seen from Fig. S4† that the oil droplet touching on the fibrous mats momentarily exhibited a spherical shape. After 1 s, the oil droplet was sorbed by the fibrous mats, displaying a collapsed shape. As time elapsed, the oil spread rapidly within the fibrous mats, filling the voids among these fibers. After 4 s, the oil was completely sorbed by the fibrous mats, showing a wet area. This process demonstrates that the as-prepared fibrous mats have a high rate of oil uptake.

Oil sorption of the composite PS–PU fibrous mats

As expected, the fibrous mats show a good hydrophobicity–oleophilicity with rapid rate of oil uptake, with the help of excellent capillary action, which makes it an idea selective sorbent for the oil spilled over water surface. Fig. S5† shows the dynamic process of the fibrous mat soaking up oil from the water surface. Several oil droplets float on the labeled water forming a thin layer of oil, which is highlighted by a red circle (Fig. S5a†). When a strip of the fibrous mat was brought into contacting with the oil layer on a water surface, the fibrous mat quickly sorbed the oil while repelling the water (Fig. S5b†). The oil wetted the fibrous mat and was retained by it after the removal of the sorbed fibrous mat (Fig. S5c†). Thus, the oil layer was successfully cleaned up from the water surface (Fig. S5d†). It can be concluded that the hydrophobic–oleophilic PS–PU fibrous mats prepared *via* co-axial electrospinning can be used as an oil sorbent to soak up oil from an oil–water environment.

In view of the hydrophobicity–oleophilicity and oil soak up ability from water surface of as-prepared fibrous mats, we investigated these fibrous mats as oil sorbents for oil sorption from a water surface. The sorption capacities of these composite PS–PU fibrous mats with regards to motor oil and sunflower seed oil are presented in Fig. 8. The sorption capacities of the fibrous mats prepared from a initial PU resin as the core solution at 20 kV (sample A) for the two kinds of oils were 54.92 and 33.23 g g^{-1}, respectively, which are much higher than the sorption capacities of conventional PP fibers for the corresponding oils (approximately 1.5–2 times that of PP fibers for these two same oils).[25] As can be seen, the sample B showed the highest sorption capacities of 64.40 and 47.48 g g^{-1} for motor oil and sunflower seed oil among all the samples, respectively. It is worth emphasizing that the composite PS–PU fibrous mats

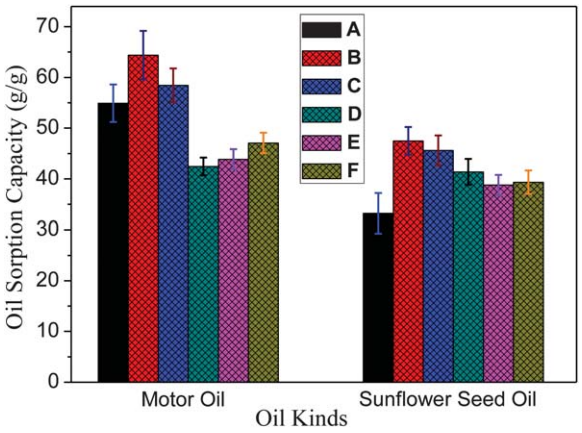

Fig. 8 Sorption capacities of the composite PS–PU fibrous mats for motor oil and sunflower seed oil. (The samples A to F are the corresponding fibers shown in Table 2.)

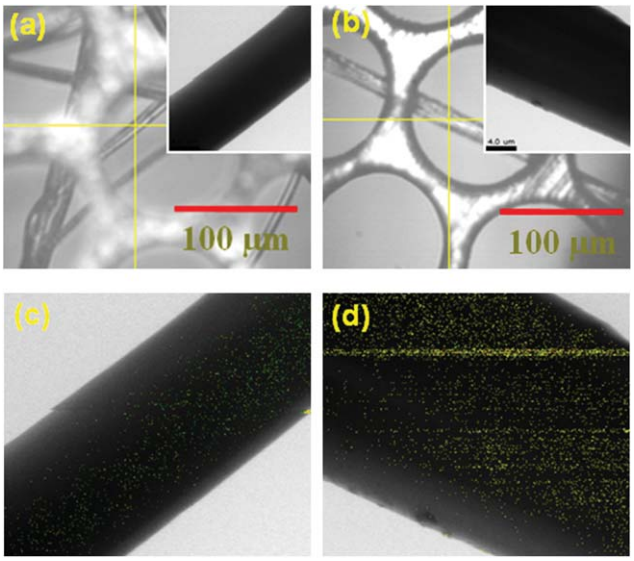

Fig. 9 Images (a) and (b) show a single composite PS–PU fiber taken from different samples shown in Fig. 2a and b, respectively, placed on the copper wire mesh after a sufficient oil sorption. (c) and (d) show the iron element distribution of the single fiber shown in (a) and (b), respectively. (The insets in (a) and (b) present the STXM images of corresponding single fiber. The crossing points of yellow lines are the positions for scan with an area of 20 × 20 μm and a smallest pixel size of 25 nm.)

prepared in one-step showed much higher oil sorption capacities compared with some surface-modified nanomaterials synthesized through a series of processing procedures, such as nanocellulose aerogels,[12] nanoparticles,[13] nanoblets[15] and nanowires.[16]

A comparison of the oil sorption capacities of sample A and sample B shows that sample B has a much higher oil sorption capacity. As shown in the previous section (Fig. 2a and b), the fibers of these two samples exhibited a very similar fiber width (or diameter). In addition, the optical images of these two samples (Fig. S6†) revealed that the fibrous mats were very fluffy, displaying a cotton-like consistency due to the different elasticities between PS and PU. Under such conditions, it is believed that a fiber with a much larger SSA and TPV will enable much more oil to be sorbed than that of a fiber with a smaller SSA and TPV.

To confirm this speculation, we investigated the comparison of oil sorption capacity for a single fiber taken from the samples A and B as presented in Fig. 9. Fig. 9a and b provide the single fiber taken from the samples A and B, respectively, after a sufficient oil (with a qualitatively traceable element) sorption. With the help of BL08U1A at the SSRF, the STXM images of corresponding fibers were obtained (insets of Fig. 9a and b). The calculated results of iron element distribution (the yellow dots represent the iron element) within the corresponding fiber were achieved as described in Fig. 9c and d, which obviously showed that the fiber with a larger SSA and TPV contained much more yellow dots, indicating that much more oil was sorbed by the fiber. Therefore, the SSA and TPV within a single fiber play an important role for its oil sorption capacity.

For an assembly of the composite PS–PU microfibers, the oil sorption mechanism can be absorption, adsorption, capillary action or a combination of these.[9,42] Firstly, the oil was sorbed by physical trapping on fiber surfaces, thus filling the inter-fiber voids. Subsequently, the oil diffused into the porous structure existing in the fibers *via* capillary action through the fiber cuticle or ends. It is reasonable that the oil sorption capacity of the as-prepared fibrous mats is dependent on the inter-fiber voids among fibers, intra-fiber porosity as well as fiber diameters. For the samples A to C, the proportion of polymer PU within the composite fibers is dominant due to the high concentration of the core solution, which enabled the fibrous mats to exhibit a cotton-like composition (very fluffy) composed of the ribbon-like fibers (Fig. 2a and b, 3a and S6†). When the 50 wt% PU resin was used as the core solution, the inter-fiber voids among these fibers were reduced due to the decrease of fiber diameter and the composition difference between PS and PU within the composite fibers. Hence, the fiber assembles of the samples D to E showed a membrane-like composition, as shown in Fig. S6,† which caused these fibrous mats to show a much lower oil sorption capacity for motor oil compared with samples A to C. This result demonstrates that the oil sorption capacity is overwhelmingly influenced by the inter-fiber voids among fibers instead of the intra-fiber porosity, which agrees with our previous study.[43]

Furthermore, it can be found that these fibrous mats showed a lower oil sorption capacity for sunflower seed oil than that for motor oil correspondingly, and there were no big difference of oil sorption capacities for samples D and E. This result was attributable to the much lower viscosity of sunflower seed oil compared with motor oil.[25,42] In the process of oil sorption, the oil with a lower viscosity can be quickly and easily moved into the inter-fiber voids and then penetrated into the interiors of fibers; however, it is also desorbed easily during the drainage period, whereas the oil with a high viscosity was not easily desorbed. Thus, these samples showed a lower oil sorption for the oil with a low viscosity. Moreover, because of the good capillary penetration ability of oil with a lower viscosity, samples D and E with a very similar SSA showed a comparable oil sorption capacity. It demonstrates that the co-axial electrospinning is an efficient way to generate typical fibrous mats for use as oil sorbents with high sorption capacities.

Oil retention of the composite PS–PU fibrous mats

When using the oil sorbents to concentrate and transform a liquid oil to a semisolid phase or to a solid state, it should be the case that the oil sorbed sorbent can be removed from the water and be handled in an appropriate manner without significant oil draining out.[44] Consequently, the oil retention of sorbent is an important factor to be considered. Fig. 10 provides the rate of motor oil desorption from the sorbed sorbent (here the sample A was selected for the investigation comparing with PP fibers) by gravity over time. As can be seen, the oil retention behaviors of the two sorbents followed almost the same trend. In the initial 10 min, the rate of oil release was very high during this period. After 10 min elapsed, the oil amounts retained by these two sorbents were 26.54 and 16.80 g g^{-1}, respectively. From the inset of Fig. 10, we observed that the amount of oil on the two sorbents decreased in the first 10 min of drainage by 52.67 and 34.12%, respectively. The result indicates that the composite PS–PU fibrous mats have a relatively poor oil retention ability compared with PP fibers due to their high porosity. Over the second stage of drainage (10–30 min), the rate of oil release was substantially reduced. After 30 min, the sorbents tended to begin a descent toward a steady state, and no significant amount of oil was drained out. Our result agreed well with the previous reports.[2,5]

Reusability of the composite PS–PU fibrous mats

Oil sorption capacities of the composite PS–PU fibrous mats (the sample A was selected for the investigation) after five cycles of the sorption process for motor oil are shown in Fig. 11. The results show that the oil sorption capacity is decreased by approximately 10.70% after the first cycle by squeezing it between two padding papers at maximum pressure to remove the sorbed oil. The oil sorption capacity decreased continuously after the second cycle and showed a value of 63.09% of its initial value; however, this did not dramatically change throughout the following sorption cycles. Even after five sorption cycles, the decrease in sorption capacity did not exceed 40% of the initial value and 35.54 g g^{-1} of sorption capacity was still maintained, which was approximately 3–5 times that of wool-based non-woven material in previous reports.[5,45] Furthermore, the decrease of oil sorption capacity was ascribable to the irrecoverable deformation and collapse of intra-fiber and/or inter-fiber pores during the process of mechanical squeezing.

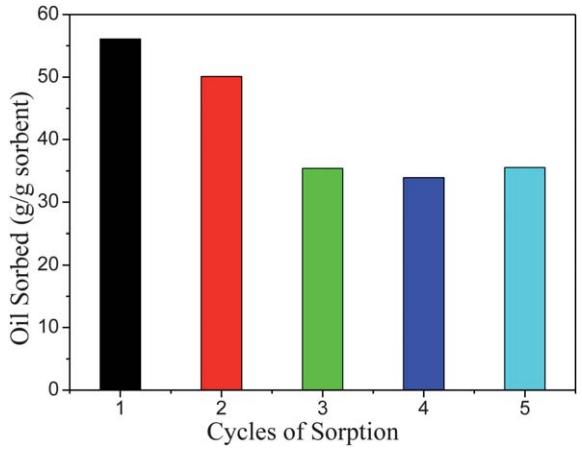

Fig. 11 Reusability of the composite PS–PU fibrous mat for motor oil.

Tensile property of the composite PS–PU fibrous mats

Although some efficient methods of oil recovery from the sorbent are available, the compression of oil sorbent is an economical and practical method. Therefore, a fairly high strength and breaking elongation, and, in particular, good shape recovery and excellent shape retention are required for the reusability of oil sorbent. Fig. 12 presents the typical stress–strain curves for the composite PS–PU fibrous mats (samples A to F). As can be noted from Fig. 12 and its inset, all the samples show a non-linear elastic behavior in the first stage due to the slip of fibers among the fibrous mats under a stress load, and then the typical stress–strain curves nearly reach a plateau. At the plateau stage, the stress was almost kept constant and the extension was increased continuously before the samples ruptured, which indicted that

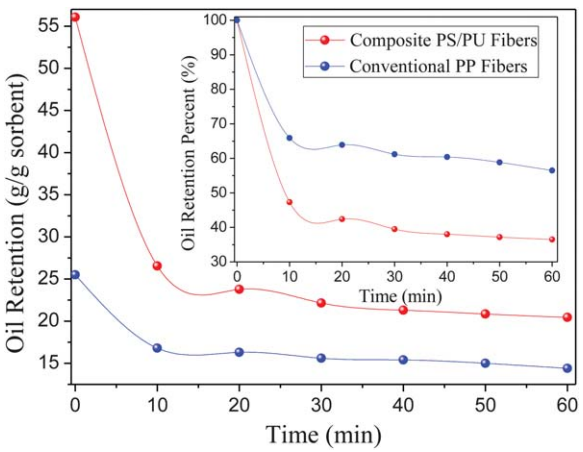

Fig. 10 Plot of oil retention on the composite PS–PU fibrous mats during free draining.

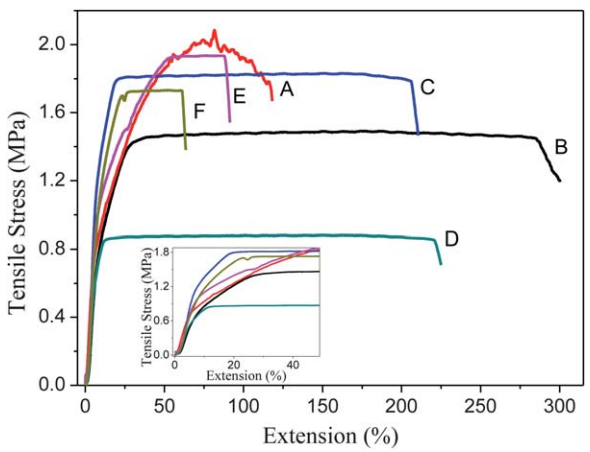

Fig. 12 Typical stress–strain curves for the composite PS–PU fibrous mats. (The samples A to F are the corresponding fibers shown in Table 2.)

the fiber slip among the fibrous mats had completed and the load was endured by the single oriented fiber along the direction of extension. The larger extension was contributed to by the addition of PU to the composite fibers.

As can be seen, sample A displays a tensile strength of 2.01 MPa and an elongation at break of 118.56% (Fig. 12). The tensile strength, elongation at break, and yield stress of the resultant fibrous mats are summarized in Table S1.† The tensile strength of the as-prepared fibrous mats was 370 times higher than that of the pure PS fibrous mats (5.45 kPa) in accordance with our previous study.[40] However, the tensile strength and elongation at break of the electrospun pure PU fibrous mats were 3.4 and 2.5 times that of the composite PS–PU fibrous mats, respectively, according to the published work.[27] Compared with sample A, sample B shows a decrease in tensile strength, which may be caused by the larger TPV within the fibers of sample B compared to sample A. A similar observation can also be found in sample D, indicating that the porous structure within the composite PS–PU fibers is adverse to the tensile strength of their assemblies. It has been demonstrated that the addition of PU to the composite fibers has significantly improved the mechanical properties which overcomes the reduction in oil sorbed fiber strength and resiliency, enabling the composite PS–PU fibrous mats to exhibit an excellent reusability.

Conclusions

In summary, we have prepared porous fibrous mats consisting of various composite PS–PU microfibers successfully *via* direct co-axial electropinning. Both BET measurements and SAXS results showed that the porous structures mainly range from 20 to 80 nm for the composite PS–PU fibers. The fine structures pertaining to fiber shape, diameter, surface morphology, interior structure as well as the SSA, TPV and APW of the as-prepared fibers can by regulated by manipulating the spinning voltages, core solution concentrations, and solvent compositions in shell solutions. The 3D fibrous mats exhibited good hydrophobicity–oleophilicity properties because of their hierarchical structures, the low surface energy and nonpolarity of PS within the composite fibers, which enabled the fibrous mats to be good oil sorbents with a relatively high sorption capacity. The results showed that the oil sorption capacities of these fibrous mats were overwhelmingly influenced by the inter-fiber voids among the fibers instead of the intra-fiber porosity. The fibrous mats showed much higher oil sorption capacities for motor oil (64.40 g g^{-1}) and sunflower seed oil (47.48 g g^{-1}), approximately 2–3 times that of conventional PP fibers for these two same oils. Even after five sorption cycles, the fibrous mats still maintained a higher oil sorption capacity. Additionally, the composite fibrous mats had significantly improved mechanical properties, which overcame the reduction in oil sorbed fiber strength, and resiliency, enabling the composite PU–PS fibrous mats to exhibit an excellent reusability.

Acknowledgements

This work is supported by the National Basic Research Program of China (973 Program, 2010CB934501, 2011CB606103, 2011CB606104, 2011CB605604 and 2012CB525005), the National Natural Science Foundation of China (no. 51173022, 10979073, 10979006 and 11005143), the "111 Project" (no. 111-2-04 and B07024), the Shanghai Committee of Science and Technology (no. 10JC1400600), the Shanghai Nano Special Projects (11nm0502900), the Innovation Program of Shanghai Municipal Education Commission (11ZZ59), the "Dawn" Program of Shanghai Education Commission (10SG32), the Scientific Research Foundation for the Returned Overseas Chinese Scholars, Ministry of Education of China, the Program for New Century Talents of the University in China, and the Fundamental Research Funds for the Central Universities. The beam time from beamlines BL16B1 and BL08U of SSRF is very appreciated. As the first author, I would like to thank Mr Quan Hu who offered me the co-axial spinneret as a gift.

References

1 T. R. Annunciado, T. H. Sydenstricker and S. C. Amico, *Mar. Pollut. Bull.*, 2005, **50**, 1340.
2 Q. Wei, R. R. Mather, A. F. Fotheringham and R. D. Yang, *Mar. Pollut. Bull.*, 2003, **46**, 780.
3 H. M. Choi and R. M. Cloud, *Environ. Sci. Technol.*, 1992, **26**, 772.
4 V. Rajakovic, G. Aleksic, M. Radetic and L. Rajakovic, *J. Hazard. Mater.*, 2007, **143**, 494.
5 M. Radetic, V. Ilic, D. Radojevic, R. Miladinovic, D. Jocic and P. Jovancic, *Chemosphere*, 2008, **70**, 525.
6 A. Bayat, S. F. Aghamiri, A. Moheb and G. R. Vakili-Nezhaad, *Chem. Eng. Technol.*, 2005, **28**, 1525.
7 Q. Wei, R. Mather and A. Fotheringham, *Bioresour. Technol.*, 2005, **96**, 331.
8 D. Ceylan, S. Dogu, B. Karacik, S. D. Yakan, O. S. Okay and O. Okay, *Environ. Sci. Technol.*, 2009, **43**, 3846.
9 H. M. Choi, H. J. Kwon and J. P. Moreau, *Text. Res. J.*, 1993, **63**, 211.
10 N. Pan, B. Wang, X. Wang and J. G. Hou, *J. Mater. Chem.*, 2010, **20**, 5567.
11 Z. Y. Zhang, R. J. Zou, L. Yu and J. Q. Hu, *Crit. Rev. Solid State Mater. Sci.*, 2011, **36**, 148.
12 J. T. Korhonen, M. Kettunen, R. H. A. Ras and O. Ikkala, *ACS Appl. Mater. Interfaces*, 2011, **3**, 1813.
13 Q. M. Pan, Q. Zhu and F. Tao, *ACS Appl. Mater. Interfaces*, 2010, **2**, 3141.
14 N. T. Cervin, C. Aulin, P. T. Larsson and L. Wågberg, *Cellulose*, 2011, **19**, 401.
15 R. Zou, Z. Zhang, L. Yu, Q. Tian, J. Wu, Y. Sun, Z. Chen and J. Hu, *Chem.–Eur. J.*, 2010, **16**, 14307.
16 J. Yuan, X. Liu, O. Akbulut, J. Hu, S. L. Suib, J. Kong and F. Stellacci, *Nat. Nanotechnol.*, 2008, **3**, 332.
17 H. W. Liang, Q. F. Guan, L. F. Chen, Z. Zhu, W. J. Zhang and S. H. Yu, *Angew. Chem., Int. Ed.*, 2012, **51**, 5101.
18 G. Wang, Q. Dong, Z. Ling, C. Pan, C. Yu and J. Qiu, *J. Mater. Chem.*, 2012, **22**, 21819–21823.
19 R. Nirmala, R. Navamathavan, H. S. Kang, M. H. El-Newehy and H. Y. Kim, *Colloids Surf., B*, 2011, **83**, 173.
20 X. F. Wang, B. Ding, J. Y. Yu and M. R. Wang, *Nano Today*, 2011, **6**, 510.

21 J. Y. Lin, X. F. Wang, B. Ding, J. Y. Yu, G. Sun and M. Wang, *Crit. Rev. Solid State Mater. Sci.*, 2012, **37**, 94.
22 J. Du, P. L. Che, Z. Y. Wang, U. Aich and K. J. Yarema, *Biomaterials*, 2011, **32**, 5427.
23 H. Zhu, S. Qiu, W. Jiang, D. Wu and C. Zhang, *Environ. Sci. Technol.*, 2011, **45**, 4527.
24 J. Y. Lin, B. Ding, J. M. Yang, J. Y. Yu and G. Sun, *Nanoscale*, 2012, **4**, 176.
25 J. Y. Lin, Y. W. Shang, B. Ding, J. M. Yang, J. Y. Yu and S. S. Al-Deyab, *Mar. Pollut. Bull.*, 2012, **64**, 347.
26 A. K. Moghe and B. S. Gupta, *Polym. Rev.*, 2008, **48**, 353.
27 R. Sen, B. Zhao, D. Perea, M. E. Itkis, H. Hu, J. Love, E. Bekyarova and R. C. Haddon, *Nano Lett.*, 2004, **4**, 459.
28 J. Y. Lin, B. Ding, J. M. Yang, J. Y. Yu and S. S. Al-Deyab, *Mater. Lett.*, 2012, **69**, 82.
29 X. Zhang, Z. Xu, R. Tai, X. Zhen, Y. Wang, Z. Guo, R. Yan, R. Chang, B. Wang and M. Li, *J. Synchrotron Radiat.*, 2010, **17**, 804.
30 A. Ziabicki, *Fundamentals of fiber formation: the science of fibre spinning and drawing*, Wiley, New York, 1976.
31 J. Y. Lin, B. Ding, J. Y. Yu and Y. Hsieh, *ACS Appl. Mater. Interfaces*, 2010, **2**, 521.
32 Y. Shin, M. Hohman, M. Brenner and G. Rutledge, *Polymer*, 2001, **42**, 09955.
33 S. Megelski, J. S. Stephens, D. B. Chase and J. F. Rabolt, *Macromolecules*, 2002, **35**, 8456.
34 L. F. Wang, C. L. Pai, M. C. Boyce and G. C. Rutledge, *Appl. Phys. Lett.*, 2009, **94**, 151916.
35 J. Y. Lin, Y. Cai, X. F. Wang, B. Ding, J. Y. Yu and M. R. Wang, *Nanoscale*, 2011, **3**, 1258.
36 B. Ding, J. Y. Lin, X. F. Wang, J. Y. Yu, J. M. Yang and Y. Cai, *Soft Matter*, 2011, **7**, 8376.
37 J. Y. Lin, B. Ding, J. Y. Yu, G. C. Wu, J. M. Yang and G. Sun, *Int. J. Nonlinear Sci. Numer. Simul.*, 2010, **11**, 523.
38 K. Sing, D. Everett, R. Haul, L. Moscou, R. Pierotti, J. Rouquerol and T. Siemieniewska, *Pure Appl. Chem.*, 1985, **57**, 603.
39 T. Narayanan, *Synchrotron small-angle X-ray scattering*, ed. R. Borsali and R. Pecora, Springer, Netherlands, 2008, pp. 899
40 X. H. Li, B. Ding, J. Y. Lin, J. Y. Yu and G. Sun, *J. Phys. Chem. C*, 2009, **113**, 20452.
41 L. D. Tijing, M. T. G. Ruelo, A. Amarjargal, H. R. Pant, C.-H. Park and C. S. Kim, *Mater. Chem. Phys.*, 2012, **134**, 557.
42 G. Deschamps, H. Caruel, M. E. Borredon, C. Bonnin and C. Vignoles, *Environ. Sci. Technol.*, 2003, **37**, 1013.
43 J. Y. Lin, F. Tian, Y. W. Shang, F. J. Wang, B. Ding and J. Y. Yu, *Nanoscale*, 2012, **4**, 5316.
44 C. P. Karan, R. S. Rengasamy and D. Das, *Indian J. Fibre Text. Res.*, 2011, **36**, 190.
45 M. M. Radetić, D. M. Jocić, P. M. Jovančić, Z. L. Petrović and H. F. Thomas, *Environ. Sci. Technol.*, 2003, **37**, 1008.